Validation of Thermal-Transport Modeling with Direct-Drive, Planar-Foil Acceleration Experiments on OMEGA

S. X. Hu,* V. A. Smalyuk, V. N. Goncharov, S. Skupsky, T. C. Sangster, D. D. Meyerhofer,† and D. Shvarts‡

Laboratory for Laser Energetics, University of Rochester, 250 East River Road, Rochester, New York 14623, USA

(Received 4 February 2008; published 29 July 2008)

We present for the first time the experimental validation of the nonlocal thermal-transport model for a National Ignition Facility relevant laser intensity of $\sim 10^{15}$ W/cm^2 on OMEGA. The measured thin target trajectories are in good agreement with predictions based on the nonlocal model over the full range of laser intensities from 2×10^{14} to 10^{15} W/cm^2. The standard local thermal-transport model with a constant flux limiter of 0.06 disagrees with experimental measurements at a high intensity of $\sim 10^{15}$ W/cm^2 but agrees at lower intensities. These results show the significance of nonlocal effects for direct-drive ignition designs.

DOI: 10.1103/PhysRevLett.101.055002 PACS numbers: 52.25.Fi, 52.57.−z, 52.65.−y

In direct-drive inertial confinement fusion (ICF), the laser energy deposited near the critical-density region is thermally transported to the ablation surface, driving the capsule implosion [1,2]. Accurate modeling of thermal transport in ICF plasmas is extremely crucial for precisely predicting laser absorption [3], shock timing [4], and Rayleigh-Taylor (RT) instability growth [5,6], all of which are essential to ICF ignition target designs. Thermal transport in laser-produced plasmas has therefore been studied intensively for the past decades [7–11]. The most widely used thermal-transport model is a local one, where the heat flux (q) generally takes the harmonic mean of the local Spitzer-Härm flux (q_{sh}) [12] and the limited free-stream flux (q_{fs}), i.e., $q = 1/[1/q_{\mathrm{sh}} + 1/(f \times q_{\mathrm{fs}})]$ [13,14]. The flux limiter $f = 0.06$, used in direct-drive ignition designs for the National Ignition Facility (NIF) [15], was inferred from glass-shell and plastic implosion experiments. Local simulations predict steep temperature and density profiles near the ablation surface at low drive intensities when the coronal temperature is below ~ 2 keV. High-intensity drives at $I \geq 10^{15}$ W/cm^2 can create much hotter plasmas with corona temperatures above ~ 3 keV. Such high-temperature conditions are relevant to direct-drive-ignition designs on the NIF. For these cases, the electrons that account for thermal transport have energies greater than ~ 10 keV and a mean free path comparable to or longer than the temperature scale length near the critical-density region. These electrons can penetrate deep into the high-density region and deposit their energy closer to the ablation surface. This effect increases the temperature and density scale lengths near the ablation surface modifying the laser absorption, shock timing, and RT instability growth.

Thermal-transport calculations based on the Fokker-Planck equation showed the importance of nonlocal electron transport even at low laser intensities of $< 1 \times 10^{14}$ W/cm^2 for drives with green ($\lambda \sim 0.53$ μm) and infrared ($\lambda \sim 1.06$ μm) lasers [16–21]. For UV lasers, with $\lambda \sim 0.35$ μm, similar simulations showed the importance of nonlocal effects at a high drive intensity of $\sim 10^{15}$ W/cm^2 [22]. Full Fokker-Planck simulations are too expensive to be routinely used to model experiments, so approximate nonlocal-transport models are developed as a compromise [23–34]. Nonlocal-transport effects were necessary to explain RT growth experiments with a green laser drive [35]. Schurtz *et al.* have recently examined nonlocal effects during the shock transit stage in thick targets using a UV laser drive [36]. Goncharov *et al.* have also demonstrated the importance of nonlocal effects to model shock propagation, unstable Ritchmyer-Meshkov growth, and cryogenic target implosions with UV drive [34,37]. Nonlocal effects were used to explain stabilization of RT growth at NIF-relevant direct-drive intensities [38]. This Letter presents for the first time the experimental validation of our nonlocal model [34,37] for the NIF-relevant drive-intensity of $\sim 10^{15}$ W/cm^2 on OMEGA using 351-nm laser light. The results show the significance of nonlocal effects for direct-drive conditions relevant to ignition on NIF.

Figure 1(a) shows a schematic of the experimental setup. In the experiments, up to ten overlapped OMEGA laser beams [39] were used to drive 20-μm-thick plastic foil. The 3×3 mm^2 CH foil was mounted on a washer with a central hole of 2.5-mm diameter. The foil was separated from the washer by ~ 50 μm. Only a central ~ 1-mm diameter part of the foil was driven. The beam configuration included two beams at 10.3° angle of incidence and four beams for each angle of incidence at 31.7° and 42.2°. Standard beam-smoothing techniques were used including distributed phase plates [40], polarization smoothing [41], and smoothing by spectral dispersion (SSD) [42]. The driven-foil trajectory was measured by a streaked camera [43] using side-on radiography as shown in Fig. 1(a), in which the Dy sidelighter was irradiated by an additional OMEGA beam. Figure 1(b) shows a snapshot of the density profile from the two-dimensional (2D) DRACO simula-

 © 2008 The American Physical Society

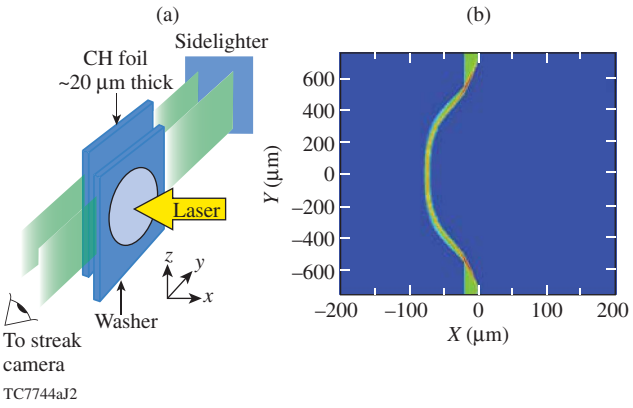

FIG. 1 (color online). (a) The schematic diagram of the experimental setup and (b) a snapshot of the density profile from DRACO simulations for a laser-driven planar foil.

tions. As the laser ablates the front surface of the CH foil, the central portion of the foil is driven along the negative x axis. The absorption of sidelighter x rays imaged the position of the driven foil.

As an example, Fig. 2(a) shows an experimental image that was taken in a shot with a 1.5-ns, shaped-pulse drive at a peak intensity of $\sim 5 \times 10^{14}$ W/cm^2. The corresponding pulse shape is plotted in Fig. 3(d). The streaked image includes driven and undriven parts of the foil and the washer below it. The temporal intensity modulation of sidelighter x rays (with a period of $\sim$100 ps) is seen in Fig. 2(a). It was caused by the SSD modulation in the drive laser intensity, as shown in Fig. 3(d). This modulation provides an accurate temporal fiducial ($\pm$20 ps), used for the on-shot temporal calibration of the streak camera. The result from postprocessing a 2D DRACO simulation of this experiment is plotted in Fig. 2(b) for the same shot. It shows the calculated absorption of sidelighting x rays as a function of position and time. The simulated trajectory reproduced the experimental features well (note that the washer is not included in our simulations). By taking the peak absorption positions as a function of time, the simulated and measured trajectories are directly compared in Fig. 3, for three different laser intensities and pulse shapes.

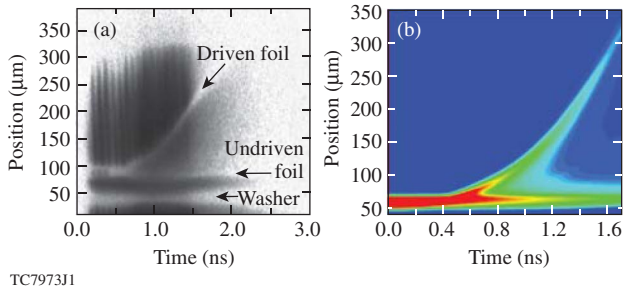

FIG. 2 (color online). The comparison of radiographic images between (a) experiment and (b) simulation for a planar foil driven by the shaped pulse shown in Fig. 3(d).

Both the standard flux limiter ($f = 0.06$) [13,14] and the nonlocal model [34,37] have been used for thermal-transport modeling in DRACO simulations. The nonlocal model solves a simplified Boltzman equation with the Krook collision operator and an appropriate electron deposition length [34,37]. It gives an effective time-dependent flux limiter $f = q_{\mathrm{nonlocal}}/q_{\mathrm{fs}}$, defined as the ratio of nonlocal heat flux to the free-streaming heat flux. Such a time-dependent flux limiter is used in DRACO simulations, and the results are compared to the modelings using a constant flux limiter of $f = 0.06$. For high-intensity drives, nonlocal thermal transport generally results in a lower coronal temperature and more laser absorption, which leads to a stronger shock when compared to the local prediction using $f = 0.06$. In postprocessing the hydrodynamics simulations, we have taken into account the temporal resolution ($\Delta t \approx 25$ ps) and spatial resolution ($\Delta x \approx 8$ μm) of the streak camera [43]. The simulated trajectories were compared to the experimental measurements as shown in Fig. 3.

In Fig. 3(a), the 2-ns, low-intensity drive at $I \approx 2 \times 10^{14}$ W/cm^2 is plotted. Figure 3(b) shows the measured foil trajectory (open circles) against the simulated results with the nonlocal model (solid red line) and the constant flux limiter $f = 0.06$ (dashed blue line). The effective time-dependent flux limiter (solid red line) from the nonlocal model is plotted in Fig. 3(c). Both the nonlocal simulation and the constant flux-limiter simulations agree with the experiment. For this low-intensity drive, the plasma coronal temperature is only about 1.5 keV, so the local transport is still applicable. For such conditions, flux limiters play an insignificant role in the driving dynamics. This is why both results are almost identical, even though the effective time-dependent flux limiter from the nonlocal calculation deviates slightly from $f = 0.06$, as shown in Fig. 3(c). A similar situation happens to the midintensity drive at peak intensity of $I \approx 5 \times 10^{14}$ W/cm^2, which is shown in the middle panels in Fig. 3. With this shaped-pulse drive, the plasma coronal temperature rises to $T \approx 2.1$ keV. Figure 3(f) shows the effective time-dependent flux limiter varying around $f = 0.06$. Nevertheless, the nonlocal model essentially gives a similar trajectory as the constant flux limiter $f = 0.06$. Both simulation results agree very well with the trajectory measurements, as illustrated by Fig. 3(e).

The nonlocal effects become important for 1-ns, high-intensity drives at $I \approx 10^{15}$ W/cm^2, which are illustrated by the bottom panels in Fig. 3. The measured trajectory (open circles) is plotted in Fig. 3(h) with both the nonlocal modeling (solid red line) and the constant flux-limiter ($f = 0.06$) simulation (dashed blue line). The nonlocal modeling agrees very well with the experiments, while the local simulation deviates significantly from measurements. For such a high-intensity drive, the plasma coronal temperature increases to above $\sim$3 keV. Since electrons accounting for

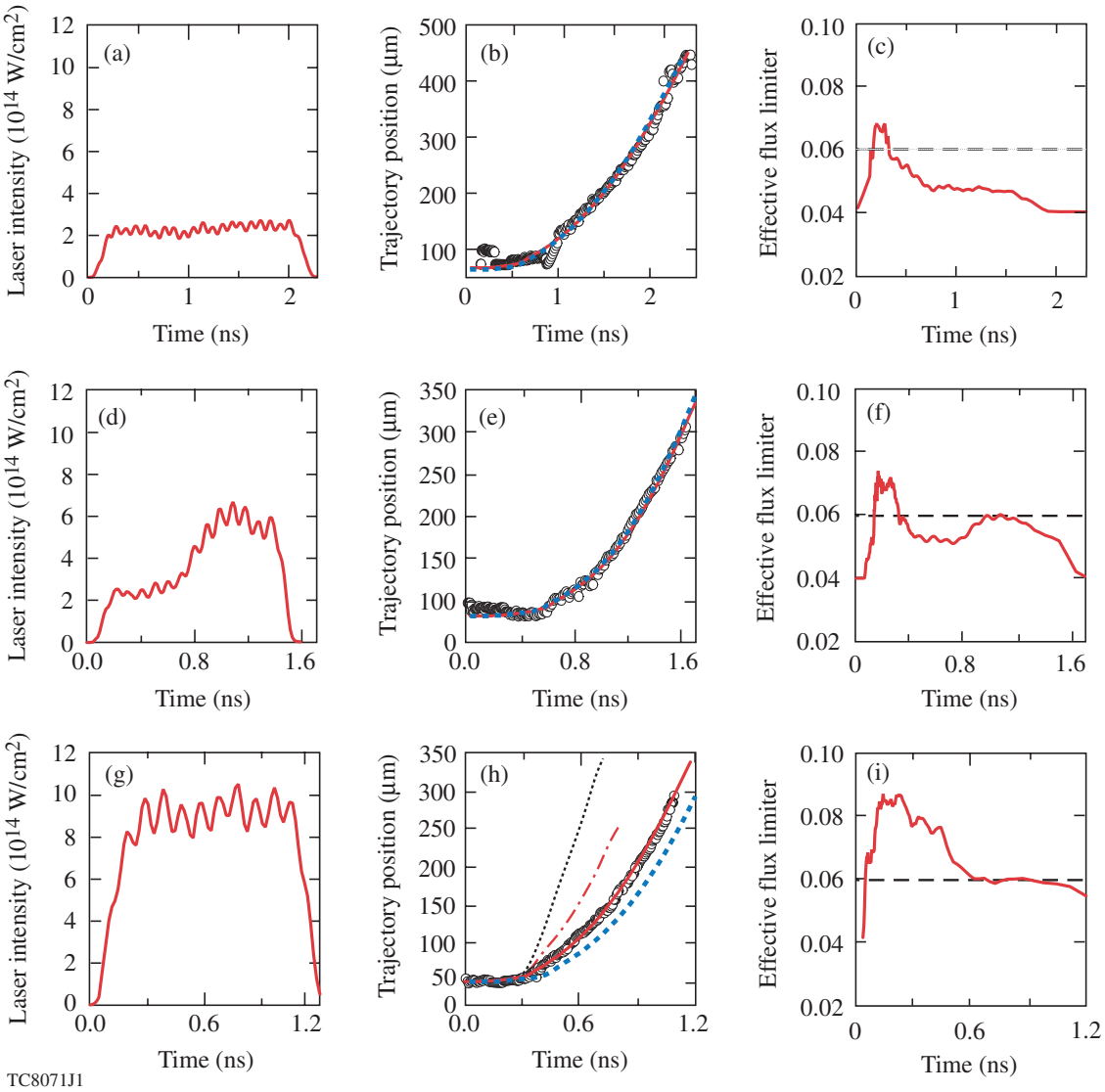

FIG. 3 (color online). Comparisons between experimental measured foil trajectories and DRACO simulations, for different laser intensities and pulse shapes: (a)–(c) the 2-ns square pulse at intensity $\sim 2 \times 10^{14}$ W/cm^2 (top panel); (d)–(f) the 1.5-ns shaped pulse at a peak intensity of $\sim 5 \times 10^{14}$ W/cm^2 (middle panel); and (g)–(i) the 1.0-ns square pulse at a higher laser intensity of $\sim 10^{15}$ W/cm^2 (bottom panel). In the central-column plots, the experimental trajectory positions are represented by open circles, while DRACO simulations are drawn with dashed blue lines for a standard flux limiter of $f = 0.06$ and with solid red lines for our nonlocal modelings. In (h), we have also included other nonlocal predictions by the dotted black line and the dashed-dotted red line, from the nonlocal models previously presented in Refs. [44] and [45], respectively.

thermal transport have a velocity ~ 2.5 times the thermal velocity [14], these thermal-carrying electrons in the plasma have an energy in the range of 15 to 20 keV. These energetic electrons in the critical-density region have a mean free path comparable to or even longer than the plasma temperature scale length. They can penetrate deeper into the ablation surface increasing the ablation velocity. Therefore, the nonlocality of thermal transport can have a remarkable consequence in the laser-target coupling dynamics for high-intensity drives. As Fig. 3(i) shows, our nonlocal modeling results in a larger, effective time-dependent flux limiter (above the nominal 0.06 value peaking at $f \approx 0.09$) during the first half of the drive, leading to stronger laser absorption since nonlocal heat transport reduces the coronal temperature. The shock launched by the laser pulse is stronger in the nonlocal modeling than in the case of $f = 0.06$. Consequently, the nonlocal simulation results in a $\sim 15\%$-higher shock speed at shock breakout, although the breakout time differs only by 20 ps between nonlocal and local simulations for such thin (~ 20 μm) targets. After the shock breaks out of the rear surface of the target, the higher initial velocity predicted by the nonlocal model is confirmed by the trajectory measurement indicated in Fig. 3(h). The target is moving

faster right after the shock breakout, which is consistent with the nonlocal modeling, while deviating from the local simulation (dashed line). The trajectory difference between local and nonlocal simulations becomes larger than ~ 50 μm at the end of the drive pulse.

Besides our nonlocal modeling, we have also included in Fig. 3(h) the predictions from two other nonlocal models previously developed [44,45]. They are plotted as a dotted black line and a dashed-dotted red line in Fig. 3(h) for the nonlocal models presented in Refs. [44] and [45], respectively. Under the small-amplitude perturbation approximation and the low-field limit, both nonlocal models expand the electron distribution function in terms of Legendre polynomials. Numerically solving the linearized electron Fokker-Planck equation and analytically fitting the simulation results, they obtained some nonlocal formulas for the thermal conductivity. For our high-intensity experiments with shocks (having density or temperature jumps), the small perturbation and low-field approximations are no longer valid; for those reasons, these nonlocal predictions do not show agreement with our experiments in Fig. 3(h). In contrast to the perturbation expansion, our nonlocal model directly solves the Boltzman equation with the Krook collision operator [34,37]. It self-consistently takes into account the electric fields associated with the nonlocal electron motion, as well as the high-field modification to the electron distribution function.

In summary, we have performed a series of planar-foil trajectory experiments on the OMEGA Laser Facility to validate thermal-transport modeling for different pulse shapes and laser intensities relevant to direct-drive ICF ignition designs. Measured target trajectories are in good agreement with predictions from the nonlocal model over the full range of laser intensities, while a local model with a constant flux limiter of $f = 0.06$ breaks down at a drive intensity of 1×10^{15} W/cm^2 but agrees with experiments at lower intensities. These results indicate that nonlocal effects are critical for direct-drive-ignition designs using high-intensity UV lasers, as to get enough implosion velocity direct-drive ignition designs are likely to have a peak laser intensity of $\sim 10^{15}$ W/cm^2 for the limited pulse duration of ~ 10 ns on NIF.

This work was supported by the U.S. Department of Energy Office of Inertial Confinement Fusion under Cooperative Agreement No. DE-FC52-08NA28302, the University of Rochester, and the New York State Energy Research and Development Authority.

*shu@lle.rochester.edu
†Also at Department of Mechanical Engineering and Department of Physics & Astronomy.
‡Also at Nuclear Research Center, Negev, Israel.

[1] J. D. Lindl, Phys. Plasmas **2**, 3933 (1995).
[2] S. E. Bodner *et al.*, Phys. Plasmas **7**, 2298 (2000).
[3] W. Seka *et al.*, Phys. Plasmas **15**, 056312 (2008).
[4] T. R. Boehly *et al.*, Phys. Plasmas **13**, 056303 (2006).
[5] H. Azechi *et al.*, Phys. Plasmas **4**, 4079 (1997).
[6] S. G. Glendinning *et al.*, Phys. Rev. Lett. **78**, 3318 (1997).
[7] W. B. Fechner *et al.*, Phys. Fluids **27**, 1552 (1984).
[8] J. C. Kieffer *et al.*, Phys. Rev. Lett. **68**, 480 (1992).
[9] A. V. Brantov *et al.*, Phys. Plasmas **5**, 2742 (1998).
[10] A. V. Brantov, V. Y. Bychenkov, and W. Rozmus, Plasma Phys. Rep. **32**, 337 (2006).
[11] D. G. Colombant, W. M. Manheimer, and M. Busquet, Phys. Plasmas **12**, 072702 (2005).
[12] L. Spitzer, Jr. and R. Härm, Phys. Rev. **89**, 977 (1953).
[13] R. C. Malone, R. L. McCrory, and R. L. Morse, Phys. Rev. Lett. **34**, 721 (1975).
[14] J. Delettrez, Can. J. Phys. **64**, 932 (1986).
[15] E. M. Campbell and W. J. Hogan, Plasma Phys. Controlled Fusion **41**, B39 (1999).
[16] E. M. Epperlein, Phys. Rev. Lett. **65**, 2145 (1990).
[17] M. Honda *et al.*, Phys. Plasmas **3**, 3420 (1996).
[18] R. J. Kingham and A. R. Bell, Phys. Rev. Lett. **88**, 045004 (2002).
[19] S. Brunner and E. Valeo, Phys. Plasmas **9**, 923 (2002).
[20] F. Alouani-Bibi, M. M. Shoucri, and J.-P. Matte, Comput. Phys. Commun. **164**, 60 (2004).
[21] A. V. Brantov *et al.*, Comput. Phys. Commun. **164**, 67 (2004).
[22] K. Otani *et al.*, Phys. Plasmas **14**, 122702 (2007).
[23] A. R. Bell, R. G. Evans, and D. J. Nicholas, Phys. Rev. Lett. **46**, 243 (1981).
[24] D. Shvarts *et al.*, Phys. Rev. Lett. **47**, 247 (1981).
[25] J. F. Luciani, P. Mora, and J. Virmont, Phys. Rev. Lett. **51**, 1664 (1983).
[26] E. M. Epperlein, G. J. Rickard, and A. R. Bell, Phys. Rev. Lett. **61**, 2453 (1988).
[27] V. Y. Bychenkov *et al.*, Phys. Rev. Lett. **75**, 4405 (1995).
[28] G. P. Schurtz, P. D. Nicolaï, and M. Busquet, Phys. Plasmas **7**, 4238 (2000).
[29] G. Gregori *et al.*, Phys. Rev. Lett. **92**, 205006 (2004).
[30] F. Alouani Bibi and J.-P. Matte, Phys. Rev. E **66**, 066414 (2002); Laser Part. Beams **22**, 103 (2004).
[31] A. Sunahara *et al.*, Phys. Rev. Lett. **91**, 095003 (2003).
[32] A. Sunahara *et al.*, J. Phys. IV **133**, 193 (2006).
[33] D. H. Froula *et al.*, Phys. Plasmas **13**, 052704 (2006).
[34] V. N. Goncharov *et al.*, Phys. Plasmas **13**, 012702 (2006).
[35] T. Sakaiya *et al.*, Phys. Rev. Lett. **88**, 145003 (2002).
[36] G. Schurtz *et al.*, Phys. Rev. Lett. **98**, 095002 (2007).
[37] V. N. Goncharov *et al.*, Phys. Plasmas **15**, 056310 (2008).
[38] V. A. Smalyuk *et al.*, Phys. Rev. Lett. **101**, 025002 (2008).
[39] T. R. Boehly *et al.*, Opt. Commun. **133**, 495 (1997).
[40] Y. Lin, T. J. Kessler, and G. N. Lawrence, Opt. Lett. **20**, 764 (1995).
[41] T. R. Boehly *et al.*, J. Appl. Phys. **85**, 3444 (1999).
[42] S. P. Regan *et al.*, J. Opt. Soc. Am. B **17**, 1483 (2000).
[43] D. H. Kalantar *et al.*, Rev. Sci. Instrum. **72**, 751 (2001).
[44] T. E. M. Epperlein and R. W. Short, Phys. Fluids B **4**, 2211 (1992).
[45] O. V. Batishchev *et al.*, Phys. Plasmas **9**, 2302 (2002).